Cement and Concrete Research 40 (2010) 763–777

Contents lists available at ScienceDirect

Cement and Concrete Research

journal homepage: http://ees.elsevier.com/CEMCON/default.asp

Temperature dependence, 0 to 40 °C, of the mineralogy of Portland cement paste in the presence of calcium carbonate

Thomas Matschei [a,b,*], Fredrik P. Glasser [b,1]

[a] Holcim Group Support Ltd, Product Innovation and Development, Im Schachen, CH-5113 Holderbank, Switzerland
[b] University of Aberdeen, Department of Chemistry, Meston Walk, Meston Building, Old Aberdeen, AB24 3UE, UK

ARTICLE INFO

Article history:
Received 28 April 2009
Accepted 21 November 2009

Keywords:
Thermodynamic Calculations (B)
Durability (C)
$CaCO_3$ (D)
Ettringite (D)
Monosulfate (D)

ABSTRACT

Thermodynamic calculations disclose that significant changes of the AFm and AFt phases and amount of Ca$(OH)_2$ occur between 0 and 40 °C; the changes are affected by added calcite. Hydrogarnet, C_3AH_6, is destabilised at low carbonate contents and/or low temperatures <8 °C and is unlikely to form in calcite-saturated Portland cement compositions cured at <40 °C. The AFm phase actually consists of several structurally-related compositions which form incomplete solid solutions. The AFt phase is close to its ideal stoichiometry at 25 °C but at low temperatures, <20 °C, extensive solid solutions occur with CO_3-ettringite. A nomenclature scheme is proposed and AFm–AFt phase relations are presented in isothermal sections at 5, 25 and 40 °C. The AFt and AFm phase relations are depicted in terms of competition between OH, CO_3 and SO_4 for anion sites. Diagrams are presented showing how changing temperatures affect the volume of the solid phases with implications for space filling by the paste. Specimen calculations are related to regimes likely to occur in commercial cements and suggestions are made for testing thermal impacts on cement properties by defining four regimes. It is concluded that calculation provides a rapid and effective tool for exploring the response of cement systems to changing composition and temperature and to optimise cement performance.

1. Introduction

The mineralogy of hydrated cement paste has long been known to be sensitive to temperature. For example, much work on delayed ettringite formation (DEF) has been concerned with curing at higher temperatures, >50 °C. Ettringite, greatly reduced in amount in the course of elevated temperature cure, reforms upon return to lower temperatures and the resulting physical expansion is detrimental to the dimensional stability of the paste matrix: an edited book gives details [1]. But—and arguably in contrast to received wisdom, holding that mineralogical changes occurring below 25 °C are negligible—the authors have encountered important mineralogical changes occurring in the lower temperature regime, 0 to 25 °C.

Relative to elevated temperature cure, rather less effort has been expended in the quantification of the mineralogical responses of hydrated Portland cement to low temperature regimes, apart from freezing, despite the fact that many concretes are either cured and used at low temperatures, or experience thermal cycling within this range in service conditions. In this context, we explore thermal/mineralogical changes but note that "low temperatures", as defined here, will exclude freezing and thawing.

The recent development of a comprehensive thermodynamic database for cement substances, embracing the temperature dependence of thermodynamic properties of the constituent phases has meant that an improved tool has become available to predict the development of paste mineralogy [2,3]. In previous publications we explored the paste mineralogy at and above 25 °C and showed that (i) with the notable exception of the metastable persistence of C–S–H and possible difficulty of nucleating and crystallising hydrogarnet, cement pastes tended to respond within days or months to reach a steady-state characteristic of the selected temperature, (ii) that sufficient data had also been generated to include all the well-known persistent metastable phases in calculations and (iii), that focussed experiments designed to check the predictive accuracy of calculations, as well as practical experience reported in the literature, support and confirm the results of calculations [2–8]. These advances have created confidence that thermodynamic calculation can rapidly and accurately predict many aspects of the mineralogical development of cement pastes. This paper presents additional data, experimental and calculated, relevant to low temperature regimes and applies calculation, supported by focussed experiment, to explore mineralogical changes. To facilitate comparison, appropriate data may be presented for somewhat higher temperatures but the main focus is on 0 to 40 °C.

* Corresponding author. Holcim Group Support Ltd, Product Innovation and Development, Im Schachen, CH-5113 Holderbank, Switzerland. Tel.: +41 58 858 64 13; fax: +41 58 858 64 09.
E-mail addresses: thomas.matschei@holcim.com (T. Matschei), f.p.glasser@abdn.ac.uk (F.P. Glasser).
[1] Tel.: +44 1224 272906.

0008-8846/$ – see front matter © 2009 Elsevier Ltd. All rights reserved.
doi:10.1016/j.cemconres.2009.11.010

2. Methods

2.1. Thermodynamic calculations

In the present study the GEM (Gibbs free energy minimisation) method included in the GEMS-PSI-code [9] was used—a software package including a GEM solver, a built-in thermodynamic standard database based on data compiled in [11–14], coupled and harmonised with a specialised database for cement substances [2,3]. Further information on the standard database, included in the current software package, GEMS version 2.2, is documented in [10]. For aqueous species, this dataset is based on the HKF (Helgeson–Kirkham–Flowers) equation of state which can be used to calculate temperature and pressure corrections up to 1000 °C and 5 kbar; the necessary parameters for aqueous species relevant for cementitious systems are given in [13,14] and are summarised in [2]. The heat capacity coefficients needed for temperature corrections for most of the minerals in the GEMS standard database are given in the *slop98.dat* dataset [12], which was originally developed for the SUPCRT92 code [12], but merged and harmonised with [11]. Raw data for cement minerals have been converted into standard molar thermodynamic properties and added to the GEMS-PSI database in order to perform modelling calculations: see [2,3]. Temperature corrections for the Gibbs energy of formation ΔG_T at the temperature of interest T of condensed substances (e.g. minerals) used in GEMS are based on the integration of the heat capacity function and are calculated according to Eq. (1) (at 1 bar reference pressure; for more details see GEMS-PSI documentation [9]):

$$\Delta G_T = \Delta_f G^0_{T_0} - S^0_{T_0}(T - T_0) - \int_{T_0}^{T}\int_{T_0}^{T} \frac{Cp}{T}\,dT\,dT \tag{1}$$

where $\Delta_f G^0_{T0}$ is the standard Gibbs energy of formation, S^0_{T0} is the standard absolute entropy both at $T_0 = 298$ K, Cp represents the heat capacity.

GEMS-PSI calculates the chemical speciation (i.e. amounts or concentrations of chemical components in all phases present at the equilibrium state) from a given total bulk composition of the system and thermodynamic data for components. Thus mass is conserved in the calculations, allowing an exact quantification of the modelled process.

The thermodynamic data of the cement-relevant phases are given in Table 1. The data are a compilation of data reported in the literature complemented by additional experiments made by the classical methods of mixing known compositions, often prepared from well-characterised phase-pure substances, made in a previous step, and again characterised after reaction by X-ray diffraction, thermal analysis, electron microscopy and chemical analysis: see previous papers for details [2,3]. It was anticipated at the outset that carbonate would have to be included as a cement component because (i) many modern cements contain calcium carbonate as a permitted additive and (ii) cements made without interground carbonate often gain carbonate at several stages: during clinker cooling, by reaction with appropriate mineral aggregates, or with the service environment, or both. The source of CO_2, as molecular CO_2 or calcium carbonate, affects mass balances differently but at low total carbonate contents the differences are slight.

2.2. Thermodynamic properties of solid solutions

Solid solutions are frequently encountered in cementitious systems. Due to the impact of solid solution on phase composition and stability, solid solutions are important and, where extensive, cannot be neglected. The molar Gibbs free energy ΔG_{ss} of a solution between different end members i can be calculated according to Eq. (2):

$$\Delta G_{ss} = \sum X_i RT\left(\frac{\Delta_f G_i^0}{RT} + \ln X_i + \ln \gamma_i\right) \tag{2}$$

where $X_i = n_i/\Sigma n_i$ (n_i is the mole amount of the end member i; $\Sigma X_i = 1$) is the mole fraction of each end member i, R is the universal gas constant ($= 8.31451$ J/(mol K), T is the temperature of interest and γ_i is an activity coefficient. Thus according to Eq. (2) the Gibbs energy of a solid solution is composed of the Gibbs energy of a mechanical mixture $\Delta_f G_i^0$ of the end members i, modified by the so-called energy of mixing ΔG_M of the solid solution series. ΔG_M can be individually computed according to Eq. (3a and b):

$$\begin{aligned} \Delta G_M &= RT\sum X_i(\ln X_i + \ln \gamma_i) \quad \text{a)} \\ &= -RT(\sum X_i \ln K_i - \ln K_{ss}) \quad \text{b).} \end{aligned} \tag{3}$$

As shown in Eq. (3b), ΔG_M can be calculated independently from the deviation of a linear function of the sum of the partial solubility products K_i of the end members i of the solid solution and the actually calculated solubility product K_{ss} of the solid solution at stoichiometric saturation, as described by Glynn [16].

Table 1
Standard molar thermodynamic properties of cement hydrates at 25 °C, 1 bar; see [2,3] for complete database.

Phase	$\Delta_f G^0$ [kJ/mol]	$\Delta_f H^0$ [kJ/mol]	S^0 [J/(mol K)]	a_0 [J/(mol K)]	a_1 [J/(mol K^2)]	a_2 [J K/mol]	a_3 [J/(mol K$^{0.5}$)]	$V°$ [cm^3/mol]	Ref
Hydrogarnet									
C_3AH_6	−5010.1	−5540	419	292	0.561	0	0	150	[1]
AFt									
C_6AsH_{32}	−15,205.9	−17,535	1900	1939	0.789	0	0	707	[3]
C_6AcH_{32}	−14,565.7	−16,792	1858	2042	0.558	−7.78e+06	0	650	[1]
AFm									
C_4AsH_{12}	−7778.5	−8750	821	594	1.168	0	0	309	[1]
C_4AcH_{11}	−7337.5	−8250	657	618	0.982	−2.59e+06	0	262	[1]
$C_4Ac_{0.5}H_{12}$	−7336.0	−8270	713	664	1.014	−1.30e+06	−800	285	[1]
C_4AH_{13}	−7326.6	−8300	708	711	1.047	0	−1600	274	[1]
C_2AH_8	−4812.8	−5433	440	392	0.714	0	−800	184	[1]
Supplementary data									
Water (H_2O)	−237.2	−286	70	75	0	0	0	18	[11]
Gypsum ($CaSO_4\,2H_2O$)	−1797.8	−2023	194	91	0.318	0	0	75	[11]
Anhydrite ($CaSO_4$)	−1322.1	−1435	107	70	0.099	0	0	46	[11]
Portlandite ($Ca(OH)_2$)	−897.0	−985	83	187	−0.022	0	−1600	33	[11]
Lime (CaO)	−604.0	−635	39	49	0.004	−6.53e+05	0	17	[11]
Calcite ($CaCO_3$)	−1129.2	−1207	93	105	0.022	−2.59e+06	0	37	[11]
Gibbsite ($Al(OH)_3$)	−1151.0	−1289	70	36	0.191	0	0	32	[11]
C_3A	−3382.3	−3561	205	261	0.019	−5.06e+06	0	89	[15]

The activity coefficient γ_i accounts for non-ideal mixing behaviour of the end members i of the solid solution series, e.g. as in the case of incomplete solid solution including the occurrence of miscibility gaps. According to Glynn [16], γ_i for a binary solid solution can be calculated from Eqs. (4) and (5):

$$\ln \gamma_1 = X_2^2[a_0 + a_1(3X_1 - X_2)] \quad (4)$$

$$\ln \gamma_2 = X_1^2[a_0 - a_1(3X_2 - X_1)]. \quad (5)$$

The empirical interaction parameters or Guggenheim parameters a_0, a_1, … are dimensionless. As shown by Glynn [17], knowledge of two fitting parameters a_0 and a_1 is sufficient to estimate the excess Gibbs energy function with reasonable accuracy.

In this study the software MBSSAS [17] was used to derive the fitting parameters a_0 and a_1 based on experimentally-observed compositional boundaries of the miscibility gap in two binary solid solution series: i) between SO_4-AFm and OH-AFm and ii) between SO_4-AFt and CO_3-AFt: a detailed description of MBSSAS is given in [17].

2.3. Modelling approach

The simplified model used here envisages a matrix composed of AFm, AFt phases, hydrogarnet (C_3AH_6), portlandite ($Ca(OH)_2$) and calcite ($CaCO_3$). Portlandite has a fixed composition and, although the amount of portlandite may vary with temperature even for a fixed bulk composition, calculations made in the course of this study will be applicable to OPC systems provided an excess is present at all times: the *amount* of excess is, however, not crucial to many calculations, those for space filling excepted. Carbonate may be present or added in the course of hydration from calcium carbonate, interground with cement or from aggregate, or from miscellaneous sources such as clinker kiln dust, or acquired by reaction with CO_2, either dissolved or gaseous, or combinations of the above. Strictly, we include only solid calcium carbonate in the scope of calculations presented here; the interaction of gaseous CO_2 with cement has been treated in [18].

Silica, a main component of Portland cement systems was omitted from the calculations, as this study focuses on the system $CaO–Al_2O_3–CaSO_4–CaCO_3–H_2O$ to highlight the temperature-dependent interactions

Side note 1

Buffer systems

The excess of portlandite buffers pH and calcium activities during initial hydration and throughout much of the service lifetime of concrete. This buffering effect limits the Ca/Si ratio of C–S–H to its calcium-saturated limit, which we believe occurs at Ca/Si about 1.6: this is somewhat lower than the generally-held limit; see the Discussion. Also, and to enable focus on conditions relevant to commercial cements, we extend the application of buffering concepts to species other than the hydrogen ion. Thus, for example, the carbonate activity—and hence the buffering activity of carbonate in cement—is typically set by the coexistence of two solid carbonate phases. Two cases can be distinguished: at low carbonate activities, the carbonate buffer pair is comprised of calcium hemi- and monocarboaluminate hydrates (shorthand, hemi- and monocarboaluminate) while at somewhat higher carbonate activities, the buffer pair is calcium carbonate and calcium monocarboaluminate. At constant temperature, either pair will jointly control the carbonate activity of the aqueous phase at the pH set by portlandite [4]. Calcium carbonate and monocarboaluminate, which are compatible phases, typically buffer the carbonate activity in cements which have been interground with calcite, or have become lightly carbonated in service, or both, provided sufficient carbon dioxide[2] is available to convert hemi- to monocarboaluminate. These reactions tend to occur at nearly constant pH as the aqueous phase in the paste is still buffered at pH ~12.5 by the presence of portlandite and C–S–H.

The buffers controlling sulfate activity are slightly more complex and depend on mass balances and reaction kinetics of the sulfates in cement. During early hydration, gypsum (or other readily soluble calcium sulfate source) effectively controls the sulfate activity but when readily soluble sources of sulfate are exhausted, as usually occurs within a few hours or days of the commencement of hydration, the paste undergoes a transition to a regime of lower sulfate activity controlled by the coexistence of AFt and monosulfoaluminate. Neither sulfate buffering reaction influences pH significantly so both reactions occur at almost constant pH because of the ongoing presence of portlandite and lime-rich C–S–H.

A characteristic of buffer systems is that they have a limited *capacity* to buffer a particular function against change. For example, if the carbonate AFm buffer system, based on the coexistence of hemi- and monocarboaluminate, is subject to ongoing reaction with added calcite; hemicarboaluminate is consumed until eventually calcite and monocarboaluminate coexist, giving rise to a second buffering pair. As it happens, the buffering carbonate activities of the two couples are numerically very close so the numerical carbonate activity increases only slightly as a consequence of the transition between the two carbonate buffer regimes. However the *capacity* of the hemi/monocarboaluminate buffer is low and the most robust of the carbonate buffer systems is comprised of the calcite–monocarboaluminate pair. Because of the large amount of portlandite resulting from cement hydration, often 20–25%, the pH of the system is also well buffered, thus fixing two of the species activities, carbonate as well as hydrogen ions. In a similar way, sulfate buffers operate mainly by the interconversion of low sulfate AFm to high sulfate AFt or *vice versa*. Because of the interference by sodium and potassium, these buffers do not have numerically fixed activities at constant temperature as would be expected from application of theory: the values are "fuzzy". However the buffer concept is a great simplification as rather few cases need to be defined in order to characterise the internal state. These cases are generic, applicable in appropriate respects to a wide range of cement compositions.

The numerical value of a particular buffer may range even at constant temperature because the solid(s) may not be of constant composition, i.e., are themselves solid solutions. But corrections for solid solutions do not invalidate the general concept. However the impact of solid solution on amounts of phase is often significant and cannot be neglected. The numerical values of the species buffering range will also be sensitive to temperature and, if hydrogen and/or OH ions are involved in buffer reactions, to pH. But the pH buffers do not involve carbonate and often operate independent, or nearly so, of buffers for anionic species such as carbonate and sulfate. For these reasons, application of buffering concepts to cement hydration greatly simplifies the number of internal states that require characterisation. This approach enables new ways of visualising and presenting data on the mineralogy and chemistry of chemically-complex cement paste systems without loss of accuracy, or need to impose arbitrary restrictions, or seriously limiting the generic applicability of the results.

[2] CO_2 dissolves in water to form hydrated CO_2 and, depending on pH, bicarbonate and carbonate ions. As a relatively rapid equilibrium exists between species under the conditions described here, we will not distinguish between speciations although the relevant computer calculations automatically assign the correct speciation.

Side note 2

Phase nomenclature

The number and compositions of phases present in a hydrated cement paste are complicated by the structural subdivision of the AFt and AFm families of phases. The system of nomenclature proposed to link structure and composition is shown in Table 2. Names are used to designate phases because names imply a specific structure, yet do not necessarily imply fixed composition. Where mineral names do not exist, i.e., where the chemical end member has no naturally-occurring equivalent, a chemical prefix is used to describe the phase, e.g., CO_3-ettringite, or carbonate-ettringite.

The AFm family of phases requires extensive subdivision because of the greater number of substitutions possible in the AFm phase of cement pastes and in the diversity of structure types: in general, mono- and divalent anions are never continuously interchangeable within an individual AFm familial member. The stacking plan of AFm phases always includes a positively charged, brucite-like layer having the composition $Ca_2Al(OH)_6^+$ (with minor Fe for Al substitution). But the layer stacking, displacement and rotation of layers with respect to a common axis, as well as the occupancy of interlayer sites potentially available for the charge-balancing anions, differ systematically with composition and structure. This is indicated, although the scheme, as developed here, does not fully take into account the range of variation possible in AFm but does cater for the operational distinctions possible by powder X-ray diffraction and allows for further subdivision, should that be desirable.

The scheme for both AFt and AFm phases does not at present distinguish between different molecular water contents because these are not always amenable to characterisation. In this study, we report the hydration state detected following drying over saturated calcium chloride at 20 °C because this degree of drying enabled contamination by atmospheric carbonation to be reduced in the course of characterisation. Work in progress on in-situ measurements, using direct examination of solids still in contact with the synthesis aqueous phase will determine the actual hydration state of AFm and AFt phases. In the absence of relevant data, we treat the loosely-bound fraction of water as having essentially the same thermodynamic properties as liquid water.

Table 2
Nomenclature for cement phases, AFm and AFt.

Familial designation	Chemical type/name[a]	Ideal formula[b]
AFt	**Ettringite**	$Ca_6Al_2(OH)_{12}(SO_4)_3\cdot 24+2H_2O$
(Al_2O_3–Fe_2O_3-tri phase)	OH-ettringite	$Ca_6Al_2(OH)_{12}(OH)_6\cdot 24+2H_2O$
	CO_3-ettringite	$Ca_6Al_2(OH)_{12}(CO_3)_3\cdot 24+2H_2O$
	Thaumasite	$Ca_6Si_2(OH)_{12}(CO_3)_2(SO_4)_2\cdot 24H_2O$
AFm	**Kuzelite = SO_4-AFm**	$Ca_4Al_2(OH)_{12}(SO_4)\cdot 6H_2O$
(Al_2O_3–Fe_2O_3-mono phase)	Hemicarboaluminate	$Ca_4Al_2(OH)_{12}[(CO_3)_{0.5}(OH)]\cdot 5.5H_2O$
	Monocarboaluminate	$Ca_4Al_2(OH)_{12}(CO_3)\cdot 5H_2O$
	Hydrocalumite	$Ca_4Al_2(OH)_{12}(OH)_2\cdot 6H_2O$

[a] Bold names and formulae are from Strunz and Nickel [37].
[b] Water content may range: see text.

between AFm and AFt phases. However work is in progress to complete the picture for silica-containing systems, including the formation of thaumasite and related solid solutions [31]. However experience has shown that formation of thaumasite in hydrated Portland cement will not occur under the limits placed on the calculations presented here. Previous studies have also shown that the calculations are unaffected by the presence of "normal" C–S–H; that is, C–S–H having a Ca/Si molar ratio ~1.6; the exact value probably lies in the range of 1.6 to 1.8, such that it also coexists with portlandite.

Iron was not included in the calculations as it was assumed that, after hydration, only small amounts appear as substituents in the main cement phases while the surplus behaves as an inert diluent, perhaps occurring as a hydrated oxide. In general, composition will be kept constant, except as noted, and the impact of thermal changes on mineralogy and volumetric relationships presented.

3. Phase assemblages containing AFt and AFm

3.1. Overview of the AFt phase: composition and characterisation

3.1.1. General review of sulfate substitution in AFt

The composition of ettringite has long been known to be variable although it is normally supposed that the composition of ettringite occurring in commercial Portland cements is close to theoretical, $Ca_6Al_2(SO_4)_3(OH)_{12}\cdot 24$–$26H_2O$. However the sensitivity limits of many microanalytical methods used to characterise ettringite in pastes, e.g. SEM or EDX microprobe analyses, preclude direct determination of OH and other substituent anions such as CO_3; this absence of total analyses has encouraged the belief that ettringite has ideal stoichiometry. Restricting the discussion to AFt in contact with portlandite, characterisation data on its composition, mainly from DTA and XRD methods, have nevertheless been variously interpreted as indicating that significant departures from theoretical sulfate content can occur. For example, the diminution of its *c*-axis spacing with time has been reported: Midgeley and Rosamon [19] attributed the diminution to increased OH substitution for sulfate while Neubauer et al. [20] attributed this trend to increased CO_3 (and ferric iron) substitution in early-formed product, with gradual replacement of these species in the course of ageing by Al and SO_4 respectively. Warren and Reardon [21] found the numerical value of the solubility product of AFt to be affected by pH and suggested that increased substitution of OH for sulfate with increasing pH was responsible. Supporting laboratory investigations also contribute evidence: Pöllmann et al. [22] and Barnett et al. [23] reported extensive miscibility between synthetic sulfate and carbonate-AFt phases, although Carlson and Berman [24] concluded that solid solution was incomplete.

On the other hand, Carlson and Berman [24] reexamined relevant samples from Flint and Wells [25], which originally contained a mix of Si-AFt and AFm, after 18 years of storage and found a single ettringite-like solid solution with complex composition, characterised by partial replacement of Al and OH by Si and CO_3 respectively, which suggests solid solution between ettringite and thaumasite. Apparently identical solid solutions were also described from natural occurrences [26–28] although an intermediate "woodfordite" composition, initially claimed to be a unique mineral species, was subsequently shown to be a carbonate- and silicate-substituted ettringite and the name "woodfordite" became discredited. It appears that "ettringite", as it occurs in Portland cement, may vary in composition and that a number of substitution mechanisms could contribute to explain the observed variations in chemistry, X-ray patterns and water contents, some of which we describe here.

To restrict the range of calculations and focus on the occurrence of these phases in Portland cement, the pH was conditioned by the presence of portlandite: the role of alkalis, which may elevate pH above this threshold, and thereby affect solubilities, phase stability and composition will be discussed subsequently. This restriction has the advantage of effectively fixing the 25 °C pH at ~12.5 i.e., the calculations apply, very nearly, to an iso-pH state leaving us free to

concentrate on hydroxide/carbonate/sulfate/silicate relationships in the AFt and AFm phases as functions of temperature.[3]

In commercial Portland cement, the carbonate activity varies between zero (no carbonate, although in practice this state is unlikely to be achieved) and an upper limit, effectively set by the solubility of calcite at the relevant pH and temperature; atmospheric CO_2 is excluded. We consider the impacts of selected substitutions in ettringite singly and in combination under these restrictions.

3.1.2. Ettringite and CO_3-ettringite

The literature [22,23] discloses that limited solid solution formation occurs between SO_4- and CO_3-AFt. Results by the authors [29] on miscibility between SO_4- and CO_3-AFt are in broad agreement with those of Pöllmann et al. [22] and Barnett et al. [23]: miscibility between the two end members is incomplete and a two-phase region occupies the range 0 to 66 mol% sulfate AFt. We observe less solid solution. Whereas data in [22,23] were obtained using the sucrose method, by precipitation of the solid solution from mixed solutions containing appropriate amounts of $NaAlO_2$, Na_2CO_3 and Na_2SO_4, giving a supersaturated lime–sucrose mixture, the present studies applied the sucrose method only to synthesise the CO_3-AFt end member, which was washed free of sucrose and subsequently mixed with SO_4-AFt in different stoichiometric amounts dispersed in pure water. This method allowed the artefact-free extraction of solubility data of the solid solutions without complexation by sucrose. The experimental data points, as mean value of several extractions, are given as markers in Fig. 1.

Stoichiometrically the dissolution of SO_4–CO_3-AFt solid solution can be described by Eq. (6):

$$Ca_6Al_2(SO_4)_x(CO_3)_{3-x}(OH)_{12}\cdot 26H_2O \rightarrow 6Ca^{2+} + 2AlO_2^- + xSO_4^{2-} + (3-x)CO_3^{2-} + 4OH^- + 30H_2O. \quad (6)$$

To obtain realistic values for the boundaries of the miscibility gap, all published data as well as solubility and solid state investigations reported by the authors [29] were taken into account but weighted towards the sucrose-free values. Thus the miscibility gap boundaries should be in the range of 0…~0.15≤x≤~1…~1.5 as defined by solutions to Eq. (6). To harmonise the available literature data with results of the present study, the miscibility gap at 25 °C was constrained to $0.12 \le x \le 1.25$ which also accounts for minor sulfate substitution in the CO_3-AFt end member. The extent of the miscibility gap with temperature will be presented in a subsequent section.

With the aid of the software MBSSAS and the known miscibility gap of the SO_4–CO_3-AFt solid solution series, the non-dimensional Guggenheim parameters, necessary to determine the excess energy of mixing ΔG_M of the solid solutions according to the algorithm given in Eqs. (3)–(5), were fitted to $a_0 = -0.823$ and $a_1 = 2.82$. With the known parameters a_0 and a_1 and the thermodynamic properties of the end members, it is now possible to recalculate the solubility data of the SO_4–CO_3-AFt solid solution series. A comparison of calculated and experimental solubility data, Fig. 1, shows satisfactory agreement. Solubilities in the region of two solid phases ($0.04 \le SO_4/(SO_4+CO_3) \le \sim 0.42$) should be constant and this is in fact experimentally observed with the result that solubility curves for each species consist of two portions: a horizontal region of constant solubility where solubility is constrained by phase rule considerations and a curved segment characterised by decreasing pH as well as by decreasing calcium and aluminium concentrations (Fig. 1a). A significant increase in aqueous sulfate concentration occurs, almost three orders of magnitude, as the composition approaches the sulfate end member of the ettringite solid solution series; note the use of a log concentration scale in Fig. 1b to encompass the wide range of concentrations.

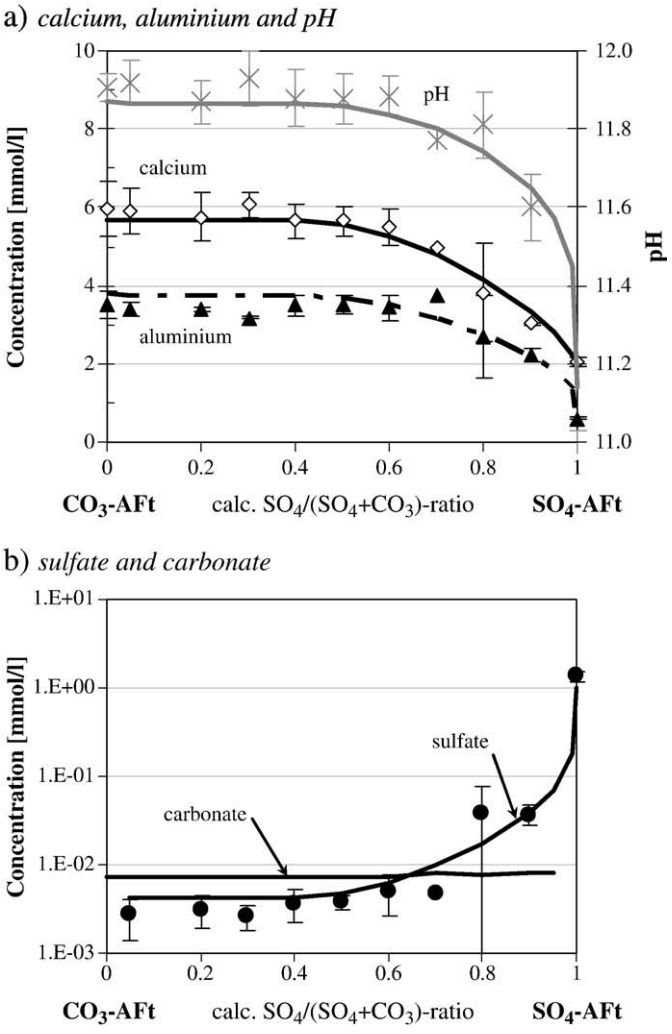

Fig. 1. Comparison of calculated (lines) and mean experimental (markers) solubilities for the SO_4-AFt and CO_3-AFt solid solution series at 25 °C (note that the calculation is restricted to SO_4–CO_3-AFt solid solutions in equilibrium with small amounts of calcite, except in the preparation of the SO_4-AFt end member).

With knowledge of the chemical composition of the solid solutions, the relative energy of mixing is calculated according to Eq. (3) by applying the Guggenheim parameters and calculating the theoretical energy of mixing using Eq. (3a), and applying the law of mass action, as stated in Eq. (3b), to the dissolution equation (Eq. (6)) and thereby calculate the relative deviation of the solubility product of a solid solution at stoichiometric saturation K_{ss} and obtain the partial solubility products of the end members, SO_4-AFt and CO_3-AFt, at given solid and aqueous solution compositions.

To minimise the systematic error resulting from analytical errors and discrepancies between the previously-derived solubility constants in the literature, K_i (Eq. (3b)) is taken to be the experimentally-derived solubility constant of end member i resulting from this study. Thus the energy of mixing of the end members becomes zero by definition and only relative changes are compared. As shown in Fig. 2, the relative changes of the theoretical energy of mixing and the values derived from the experiments are in agreement, which supports the applicability of the solid solution model and its accuracy. Both curves display a similar curvature and pass through a minimum between

[3] But pH cannot be compared directly across a range of temperatures. The neutral point, defined in terms of the ion product of water, is temperature dependent and at constant pressure, the numerical value of Kw changes to reflect increasing dissociation with rising temperature. Hence the neutral point, pH 7 at 25 °C, is not a constant except under the defined conditions.

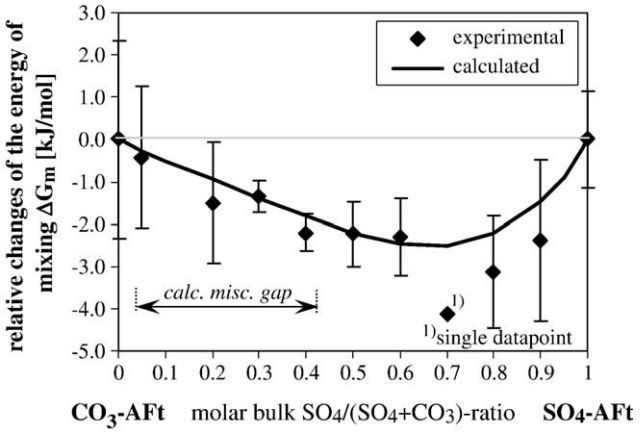

Fig. 2. Comparison between calculated and experimentally-derived changes of the relative energy of mixing of the SO_4–CO3-AFt solid solution series at 25 °C.

$SO_4/(SO_4+CO_3)$ ~0.6 to ~0.8, which corresponds to the maximum driving force of solid solution formation between the two end members. The mean experimental values at $SO_4/(SO_4+CO_3)=0.7$ to 0.9 are slightly lower than calculated but the deviations from the theoretical curve lie within the analytical errors.

The previous pure-phase experiments and calculations indicated that the AFt phase can be stabilised by the substitution of carbonate in its structure. Consequently the following calculations were used to assess the implications of carbonate substitution for phase assemblages relevant to hydrated carbonate-containing Portland cements: the relevant thermodynamic data are given in Table 1.

A theoretical composition of 1 mol $Ca_6Al_2(SO_4)_x(CO_3)_{3-x}OH_{12}\cdot 26H_2O$ (with $0\leq x\leq 3$) was equilibrated with 1.5 mol portlandite and 1 kg H_2O (pH buffered by portlandite to 12.48). The calculated mass balance changes are shown in Fig. 3 as functions of carbonate/sulfate ratio. A maximum of 9 mol% substitution of sulfate by carbonate will occur when the pH is buffered by portlandite and the carbonate activity is buffered by the coexistence of calcite and monocarboaluminate at 25 °C: the carbonate activity of the buffer pair is thus insufficient to stabilise carbonate-AFt but will support a SO_4–CO_3-AFt solid solution with a $CO_3/(SO_4+CO_3)$ ratio ~0.09. Thus the maximum amount of ettringite is not limited by sulfate content alone.

The influence of temperatures <25 °C was investigated by using the previously-derived solid-solution model for SO_4–CO_3-AFt. The results of the calculation should be regarded as tentative, as we estimated the thermodynamic data for CO_3-AFt and related solid solution from extrapolation of isothermal results obtained at 25 °C (see [2]). Restricting the assessment to the carbonate activity conditioned by the buffer pair (calcite and monocarboaluminate), calculation discloses that temperature has a significant impact on the upper limit of carbonate solid solution in AFt. Fig. 4 shows the calculated maximum extent of carbonate substitution at calcite saturation and the pH conditioned by portlandite; carbonate substitution is calculated to increase rapidly with decreasing temperature. We have shown experimentally that if mixtures of C_3A, $CaSO_4$ and $CaCO_3$ are equilibrated at 5 °C and 25 °C, with formation of AFt, substantially more calcite is dissolved in the AFt structure at 5 °C relative to 25 °C, thus confirming qualitatively the enhanced solubility of carbonate in ettringite resulting from relatively small temperature differences, in this example, between 25 and 5 °C [30]. The saturation is predicted to reach about 33% CO_3-AFt at 5 °C and increase to ~50% at 0 °C. Experimentally, carbonate saturation of the AFt phase occurs relatively rapidly at 5 °C, within a few weeks, despite the low aqueous carbonate activity conditioned by the joint solubility of calcite and monocarboaluminate. While the solubility of calcite also increases with decreasing temperature in this range, the increase is slight, only a few %, and cannot be completely responsible for the rapid disappearance of calcite.

3.1.3. Ettringite and thaumasite

No study of the AFt family would be complete without including thaumasite. Indeed, more data to the temperature-dependent solubility of thaumasite have been accumulated. But the data necessary to perform calculations require special treatment in order to interface them with data for other cement solids and will be described in a separate paper [31]. However, thaumasite, with its distinctive silica content, will not be stable in unaltered Portland cement at any temperature.

3.2. AFm relationships

3.2.1. Monosulfoaluminate in the system $CaO–Al_2O_3–CaSO_4–H_2O$

Portland cement systems characteristically contain sulfate and the affinity of sulfate for the AFm phase in preference to hydroxide stabilises the AFm structure [4]. In a cement environment, the relative activities of hydroxide and sulfate are such that hydroxide partly replaces sulfate in “sulfate”-AFm, giving rise to a range of solid

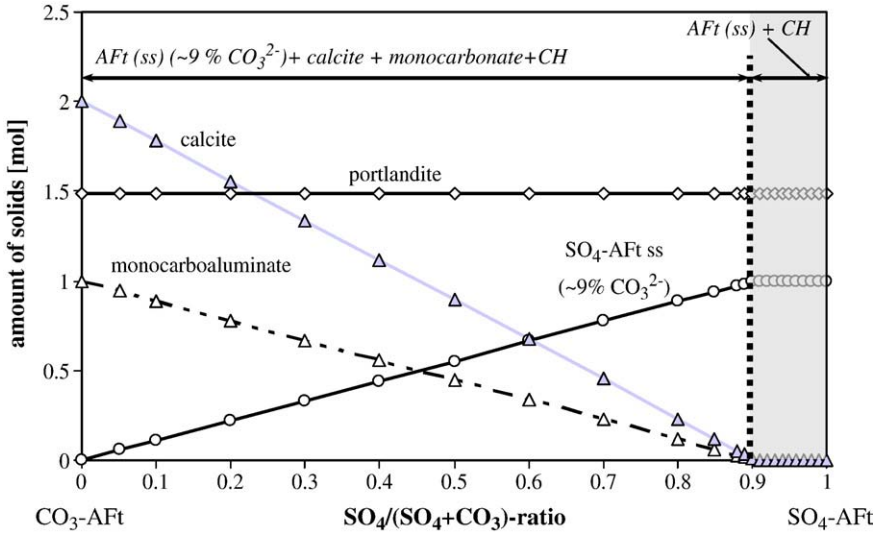

Fig. 3. Calculated stable assemblages in the (SO_4–CO_3)-AFt system buffered by excess portlandite at 25 °C.

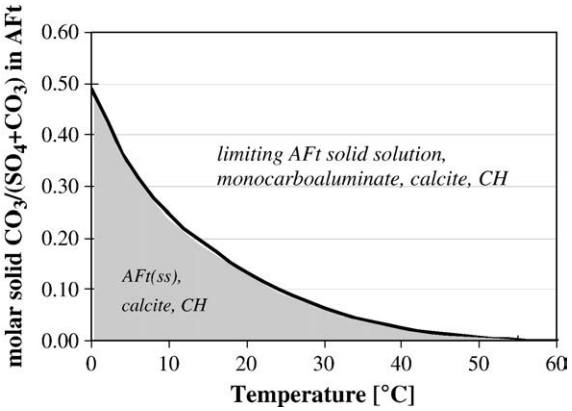

Fig. 4. Calculated maximum carbonate substitution in AFt (heavy curve) as a function of temperature; the AFt phase is equilibrated with excess calcite, monocarboaluminate, portlandite and (not shown) an aqueous phase.

solutions extending from SO_4-AFm to a maximum of about 50% replacement of sulfate by OH at 25 °C. The partial substitution, of OH for SO_4, is economical of sulfate: the amount of nominally SO_4-AFm is not necessarily limited by total sulfate. As we will show, the composition of "SO_4-AFm" is very temperature dependent. To progress calculations it is necessary to have additional data.

In agreement with experimental data [4] and literature data by Roberts [33] and Pöllmann [32], ~50 mol% of sulfate in the monosulfoaluminate phase can be replaced by hydroxide at ~25 °C. The dissolution reaction for the non-ideal monosulfoaluminate–hydroxy-AFm solid solution series is shown in Eq. (7):

$$Ca_4Al_2(SO_4)_x(OH)_{14-2x}\cdot 6H_2O \rightarrow 4Ca^{2+} + 2AlO_2^- + xSO_4^{2-} + (6-2x)OH^- + 10H_2O. \quad (7)$$

The experimental investigations agree with calculation concerning an apparently non-ideal mixing behaviour of SO_4-AFm and OH-AFm, characterised by a miscibility gap in the range of $0.03 \le x \le 0.5$ at 25 °C. Whereas the upper limit of the miscibility gap at a maximum hydroxide substitution of 50 mol% in monosulfoaluminate was confirmed by experimental investigation the lower limit was estimated according to the best fit of the solubility data (see below) and to account for the known small (<5%) sulfate incorporation in the OH-AFm end member.

By applying the non-ideal solid solution model described previously the thermodynamic properties of the solid solutions were estimated. As described above, the software MBSSAS was used to determine the non-dimensional Guggenheim parameters a_0 and a_1, necessary to calculate the activity coefficients γ_i of the end members according to Eqs. (4) and (5). By using the experimentally determined limits of the miscibility gap, $0.03 \le x \le 0.5$, and Eq. (7), the Guggenheim parameters were calculated to be $a_0 = 0.188$ and $a_1 = 2.49$.

As shown in Fig. 5, comparison between experimentally-derived solubility data and calculated solubilities of the monosulfoaluminate–hydroxy-AFm solid solutions at 25 °C shows excellent agreement in the range of $0.05 \le SO_4/(SO_4 + 2OH) \le 1$, which accounts for the good internal consistency of the dataset. The aqueous pH and solubilities of Ca and Al remain approximately constant in the region of coexistence of two solid phases, as predicted from theory. Sulfate solubilities are shown separately, in the right-hand portion, because the low numerical values of sulfate solubility require a different scale. However the limit of analytical sensitivity for sulfate was about 2 μM and only sulfate-rich compositions gave solubilities within the analytical range. The data are however sufficient to extend the values for sulfate solubilities by calculation. The solubility data obtained in this way for the pure OH-AFm end member differs significantly from calculated values. The differences can be reconciled by noting that in the solubility calculation, shown in Fig. 5, the metastability of C_4AH_x with respect to C_3AH_6 and portlandite was suppressed. However experiments show that C_4AH_x rapidly decomposes to the latter phases at 25 °C; its partial decomposition is believed to be responsible for differences between calculated and experimental data. As decomposition only affects the sulfate-free composition, C_4AH_x, this was interpreted as additional evidence for stabilisation of the OH-AFm end member by substitution of small amounts of sulfate in its structure.

With the help of previously determined solubility data (see Fig. 5) the experimentally-derived energy of mixing was calculated as described above according to Eq. (3a and b). Apart from the value at $SO_4/(SO_4 + 2OH) = 0.90$, the experimentally-derived and theoretically calculated energies of mixing are in good agreement (Fig. 6). The negative deviation from zero corresponds to the thermodynamic stabilisation energy achieved by substitution of OH in the SO_4-AFm type structure. While the numerical value of the stabilisation energy is not large, not exceeding approximately 2 kJ/mol, it is significant in the present context because it results in the greater stability of (SO_4,OH,)-AFm solid solutions, relative to expectations based on data for pure SO_4-AFm and assuming ideal mixing with OH-AFm. As will be shown subsequently, the non-ideal nature of these AFm solid solutions also affects anion partition generally and hence AFt–AFm phase relationships.

The extent of solid solution in SO_4-AFm and its coexistence with other phases are strongly temperature dependent. Fig. 7 has been

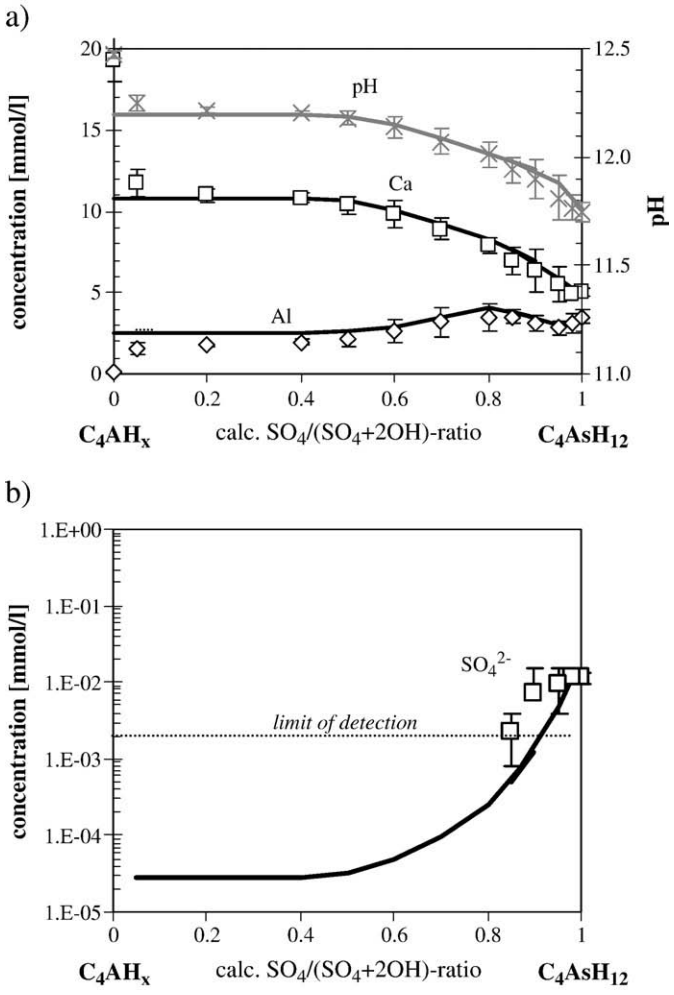

Fig. 5. Comparison of calculated (lines) and mean experimental (markers) solubility data for the SO_4-AFm and OH-AFm solid solution series at 25 °C.

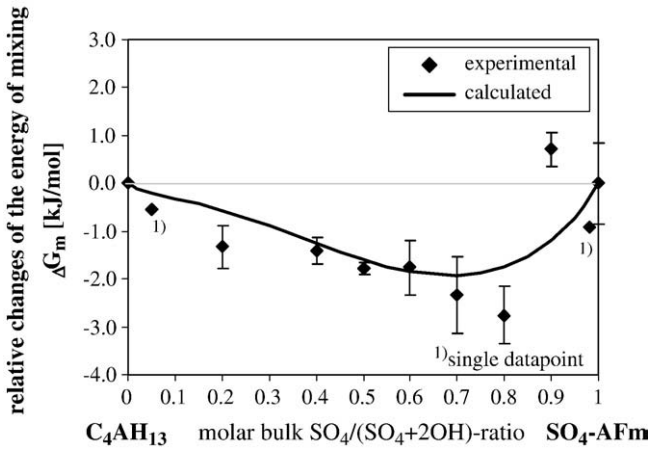

Fig. 6. Comparison between calculated and theoretical changes of the relative energy of mixing of the SO_4–OH-AFm solid solution series at 25 °C.

constructed as a guide to show this dependence; it is termed a "finder" diagram. The chemistry of AFm and its coexistence with other phases are depicted as functions of molar SO_3/Al_2O_3 ratio and temperature. A scale at the right-hand side shows the composition of the AFm phase while the central portion of the diagram shows the coexistence of AFm with other phases. Portlandite is presumed to be in excess but the amount of excess is not crucial to the construction, although it affects phase amounts. The shaded area represents the range of SO_4-AFm solid solution compositions (shorthand, Ms), whereas the composition of monosulfoaluminate in the un-shaded regions is fixed according to the temperature and initial SO_3/Al_2O_3 ratio. The stable range of OH-AFm existence is confined to a small rectangular region at low temperatures, <8 °C, and low, <0.5 (SO_3/Al_2O_3) ratios but throughout most of the temperature range, SO_4-AFm solid solutions occur as a thermodynamically stable phase.

Guidance for the interpretation of Fig. 7 is provided by an example. A dashed construction line has been added at 25 °C from which the AFm phase composition can be predicted by extending a horizontal construction line to its intersection with the right-hand scale. The monosulfoaluminate phase can thus have a composition at either points A or B, or an intermediate composition between A and B, depending on bulk composition, as defined by the sulfate ratio. Whereas point A represents the stable composition for monosulfoaluminate in equilibrium with C_3AH_6, portlandite and aqueous solution, point B gives the composition for monosulfoaluminate in equilibrium with AFt, portlandite and aqueous solution. From the resulting intersections at A and B one can now determine the composition, i.e. the $SO_4/(SO_4+2OH)$ ratio of the monosulfoaluminate solid solution by constructing a horizontal line to the right-hand scale. Thus at 25 °C monosulfoaluminate will have a constant lower limiting $SO_4/(SO_4+2OH)$-ratio ~0.76 in its equilibrium with C_3AH_6, portlandite and aqueous solution but will have a limiting $SO_4/(SO_4+2OH)$-ratio ~0.9 if it is in equilibrium with AFt, portlandite and aqueous solution.

Other conditions can be treated in the same way. An important generalisation is that, with rising temperature, the range of monosulfoaluminate compositions encountered in cement narrows and approaches more closely that of ideal monosulfoaluminate. Conversely, at lower temperatures, potential for formation of SO_4-AFm is not necessarily limited by sulfate content because significant and increasing replacement of sulfate by hydroxide can occur.

Another way of depicting the phase relationships is in terms of the specific volume of solids as a function of temperature. Due to different densities of the hydrate phases, the temperature-dependent phase changes will influence the space-filling properties of the hydrated cement paste. Fig. 8 shows a specimen calculation for a composition formulated from 1 mol each of C_3A and $CaSO_4$ and 1.25 mol $Ca(OH)_2$, reacted with 500 g water: calculations for other ratios of components have generic similarities to the example shown, provided water is present in excess. The molar volume of the equilibrium solids is shown as a function of temperature. Note that the total specific volume of solids increases with decreasing temperature. While the $SO_4/(SO_4+2OH)$ ratio of monosulfoaluminate decreases (see inset to Fig. 8), sulfate thus displaced from AFm reacts with formation of additional AFt. The AFt, in turn, increases the total specific solid volume at temperatures <~55 °C. The numerical values of maximum volume as a function of temperature are of course affected by the sulfate ratio but sensitivity studies disclose a generic conclusion: that maximising the amount of AFt also maximises the space filling by solids. The calculation is not corrected for thermal dilational coefficients but the correction is negligible, given the short range of temperatures.

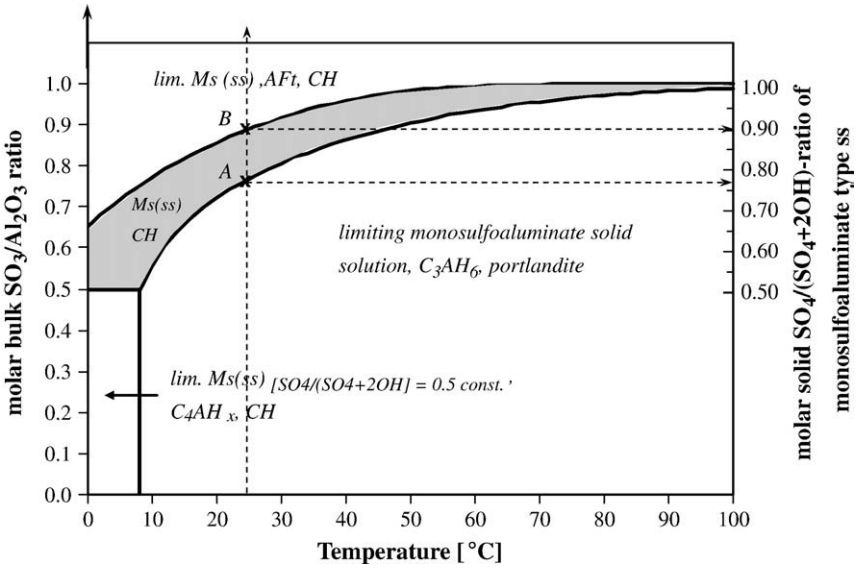

Fig. 7. Calculated maximum amount of hydroxide substitution in monosulfoaluminate as a function of temperature.

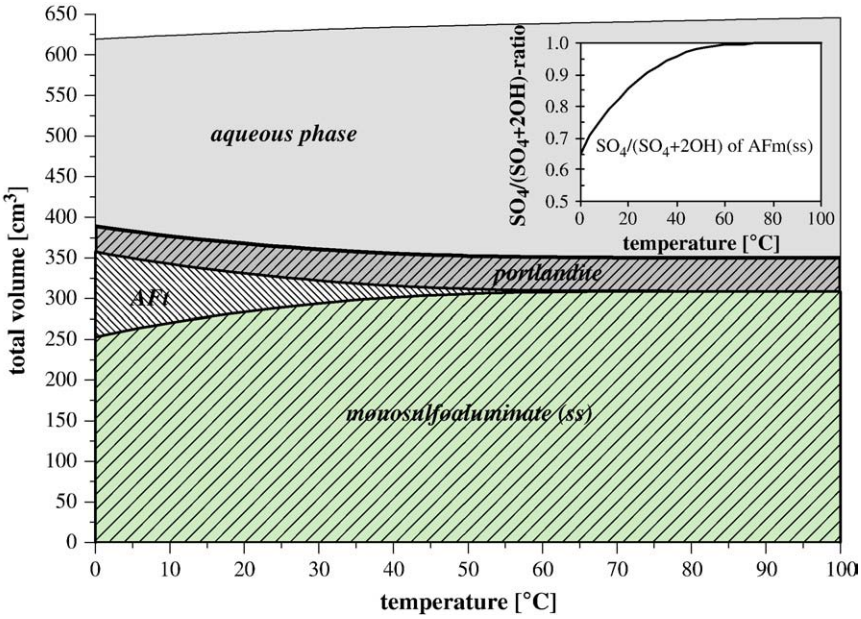

Fig. 8. Specific volume changes of a mixture of $C_3A + CaSO_4 + Ca(OH)_2$ ($SO_3/Al_2O_3 = 1$; total amount of solids = 3.25 mol) reacted with 500 g water as a function of temperature.

3.2.2. Carbonate-AFm and the system $CaO–Al_2O_3–CaCO_3–H_2O$

The temperature dependence of the AFm system in respect of saturation with respect to calcite is shown in Fig. 9. The diagram usefully outlines the division between reactive calcite and free calcite; calcite saturation is not achieved except at carbonate ratios >1.0 up to 84 °C. However, the binding of calcite into aluminates is complex; moreover the hemicarboaluminate phase has a limited thermal stability and is not calculated to be stable at >52 °C while carbonate-free C_4AH_x is only stable at low carbonate ratios and low temperatures, <8 °C. The diagram also shows how carbonate suppresses the stability of hydrogarnet as a stable phase. The stability of hydrogarnet in the lime–alumina–water system relative to AFm has long been known and the non-appearance of hydrogarnet in Portland cement paste has been attributed to kinetic factors: of the difficulty to nucleating the physically-dense hydrogarnet. However calculations underlying Fig 9 show that chemical reasons exist why C_3AH_6 does not appear: it is never stable below about 8 °C and in the range between 8 and 52 °C, it is only stable in the presence of excess portlandite at low carbonate ratios. However with rising temperature, the hydrogarnet stability field expands to higher carbonate ratios in stepwise manner until above 84 °C, hydrogarnet becomes stable at all carbonate ratios.

Thus in normal Portland cement pastes, a temperature-dependent competition for carbonate occurs between AFm and AFt phases but more generally, competition for anion sites arises from the simultaneous presence of hydroxide, sulfate and carbonate. To explain this competition fully, we have to examine AFm–AFt phase relationships.

3.3. AFt–AFm phase relationships

3.3.1. General relations

A previous version of the AFm–AFt phase relationships at 25 °C has been presented [4] but requires modification to take into account the

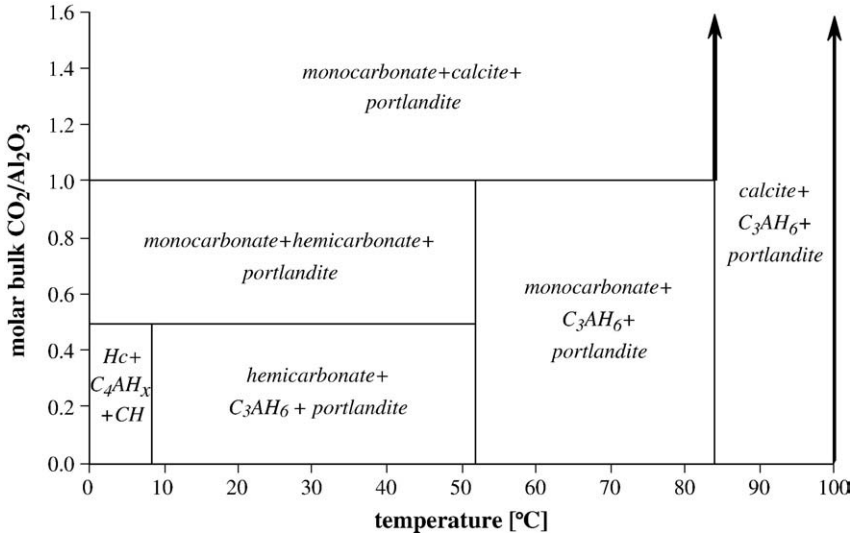

Fig. 9. Phase diagram system $CaO–Al_2O_3–CaCO_3–H_2O$ (at portlandite saturation).

solid solution of carbonate substitution into nominally SO_4-ettringite and the revised phase relationships amongst the AFm phases. Fig. 10 shows the calculated phase relationships at three selected temperatures: a) 40 °C, b) 25 °C and c) 5 °C. The compositions of most of the constituent solids project along the edges of the diagram: hemi- and monocarboaluminate on the horizontal axis and monosulfoaluminate (AFm) and trisulfoaluminate (AFt) on the vertical axis.

If we first consider the mineral composition of cements either free of carbonate, or containing only traces of carbonate, their compositions project on or close to the left-hand edge of the diagram, Fig. 10, so that the AFm/AFt mineralogy is determined primarily by the sulfate:alumina mass ratio (termed the "sulfate ratio"). The diagram does not show the proportions of phases but except for the products of incongruent breakdown, these proportions can readily be calculated by application of the lever rule to Fig. 10. Thus at 40 °C, Fig. 10a, zero carbonate and $SO_3/Al_2O_3 = 1.0$, the AFm/AFt mineralogy will project at the termination of the boundary between regions VII and VIIIa and consist of monosulfoaluminate only (an excess of aqueous phase, not shown, is presumed always to be present). On the other hand, if the molar bulk ratio of CO_2/Al_2O_3 is allowed to increase at the same sulfate ratio, 1.0, an excess of AFt will develop: the three solids of region VII will form in response to changing composition. Even when

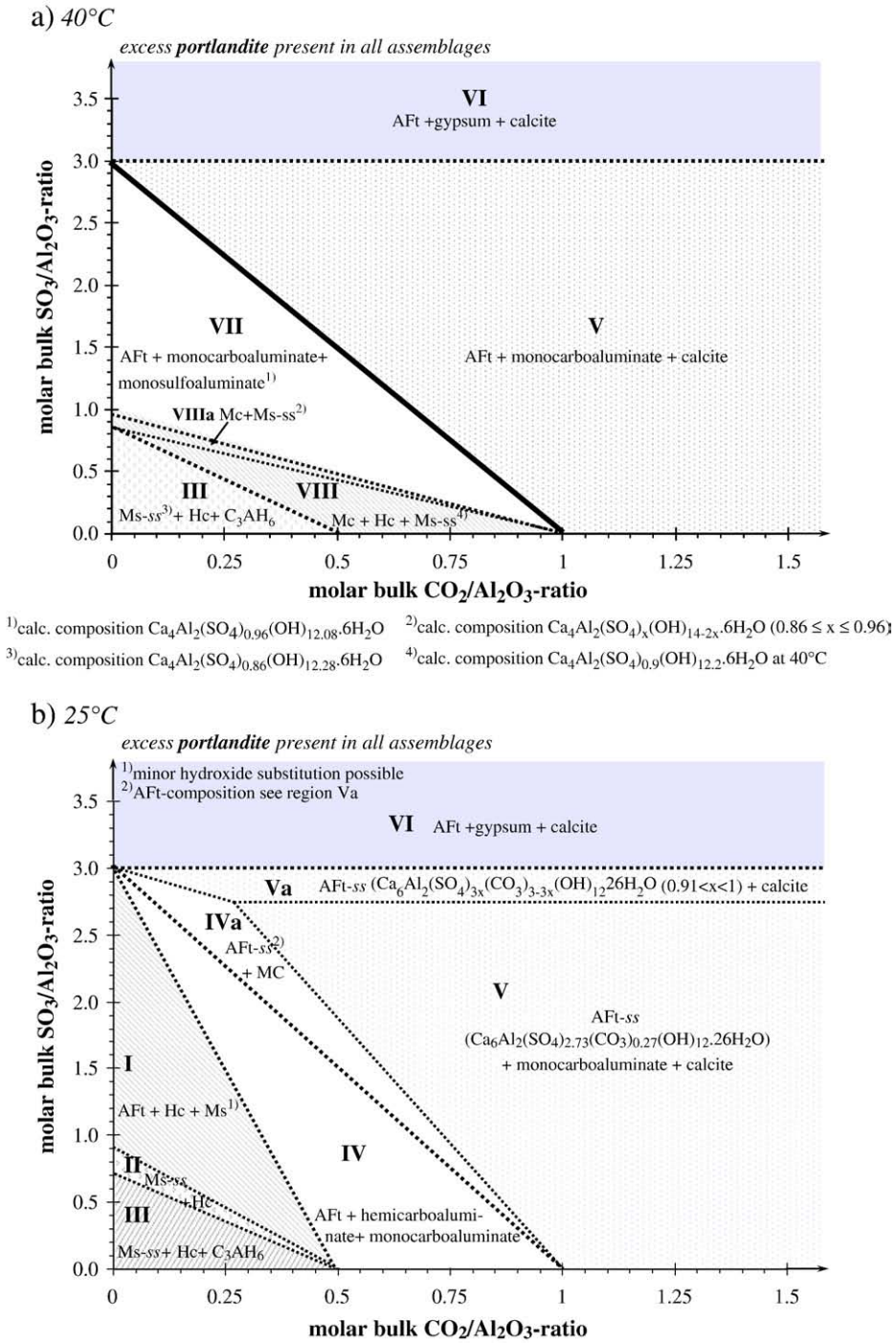

Fig. 10. Calculated phase assemblages of a hydrated mixture consisting of C_3A, portlandite and varying initial sulfate (SO_3/Al_2O_3) and carbonate contents (CO_2/Al_2O_3) at 5, 25 and 40 °C (including SO_4–CO_3-AFt solid solutions).

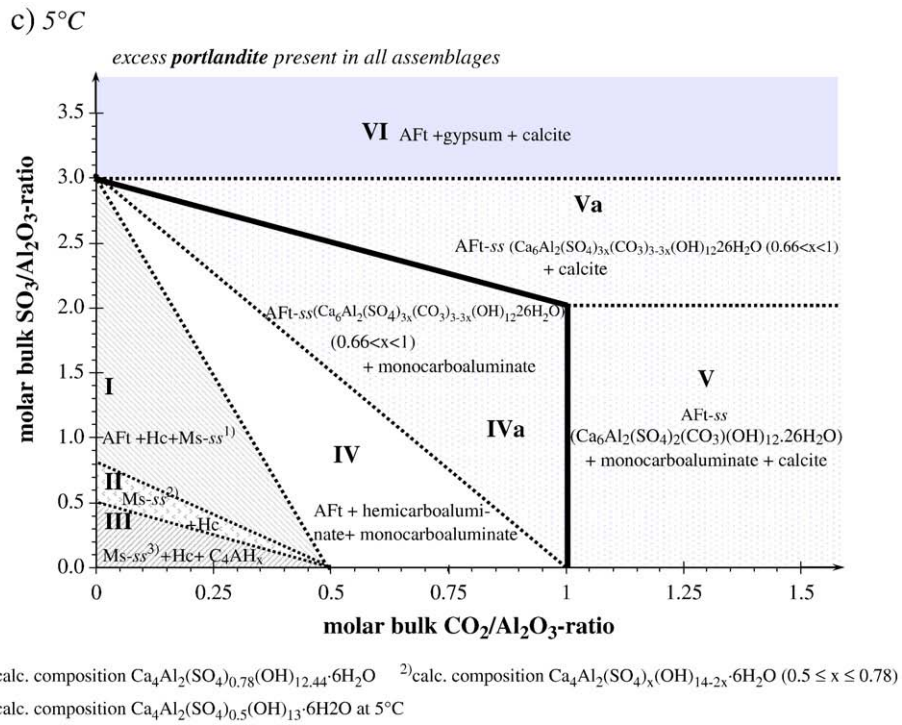

Fig. 10 (*continued*).

compositions are oversaturated with respect to calcite, such as those in region V, ettringite will still have close to its theoretical composition because of the instability of carbonate substitution into AFt at elevated temperature: the equilibrium overwhelmingly favours fractionation of carbonate into monocarboaluminate, any excess over that required to form monocarboaluminate appearing as calcite.

The diagram for 40 °C, shown in Fig. 10a, is the simplest to analyse with respect to the constitution of the AFt and AFm phases, both of which closely approach their theoretical compositions at this temperature (see Table 2). However at lower temperatures, <40 °C, the extent of hydroxide substitution in monosulfoaluminate increases significantly. Most commercial cements contain sufficient sulfate to stabilise an AFm composition close to monosulfoaluminate if cured at 40 °C but at lower temperatures, the trend to more extensive substitution of OH for sulfate stabilises AFm with respect to hydrogarnet.

If we contrast data for 40 °C with those for 5 °C, Fig. 10c, three important differences occur. Firstly, the greater stability with decreasing temperature of hydroxide-substituted AFm phases eliminates the occurrence of hydrogarnet as a stable phase. In agreement with the literature, C_4AH_x has a stability field at 5 °C. Secondly, the stability domain of hemicarboaluminate increases with the result that the positions of phase boundaries shift drastically with respect to their position at higher temperatures. As expected, increasing carbonate activity favours conversion of OH-AFm first to hemi- and finally to monocarboaluminate but only monocarboaluminate can coexist with excess calcite. Finally, the domain of ettringite compositions greatly expands to embrace an extensive range of carbonate-containing compositions, resulting in creation of region IVa and creation of a new region, Va, so that at 5 °C up to 1/3 of the sulfate in the idealised AFt composition may be replaced by carbonate. On the other hand, essentially no carbonate substitution in AFt is predicted in regions I–IV, Fig. 10c, due to very low carbonate activities prevailing in these regions. Monocarboaluminate and partially carbonate-substituted SO_4–CO_3-AFt coexist until the phase boundary between regions IVa and V (at SO_3/Al_2O_3 ratios ≤ 2 and $CO_2/Al_2O_3 = 1$) is crossed: thus the heavy lines separating region IVa from regions V, Va and VI mark the saturation limit of calcite. Note that the position of the calcite saturation limit is also sensitive to the sulfate ratio, but only at sulfate ratios >2.0; at ratios <2.0, its position is insensitive to the numerical value of the sulfate ratio. Monocarboaluminate becomes unstable in region Va at SO_3/Al_2O_3 ratios >2. Under these conditions, all alumina is bound in the AFt phase and no alumina is available to form monocarboaluminate. Thus SO_4–CO_3-AFt with varying carbonate contents (decreasing carbonate substitution with increasing SO_3/Al_2O_3) coexists with calcite and portlandite in region Va.

Fig. 10b shows the phase relations at an intermediate temperature, 25 °C, revised from previously published results to include SO_4–CO_3-AFt solid solutions. Carbonate substitution in AFt is not extensive but reaches its maximum when AFt coexists with monocarboaluminate, calcite and portlandite in region IVa. In general the calculations have shown that the amount of carbonate that can be absorbed by cement solids before calcite saturation is achieved will increase rapidly with decreasing temperature.

3.3.2. Specimen calculations

The impact of changing temperature on specific volume of the solids can be demonstrated as follows. A model cement composition was formulated from a mixture of C_3A, calcium sulfate ($SO_3/Al_2O_3 = 1.0$), calcite ($CO_2/Al_2O_3 = 1.25$) and portlandite. The model composition used for calculation thus corresponds to 0.722 mol each of $CaSO_4$ and C_3A, 0.9035 mol of calcite, 0.9025 mol of $Ca(OH)_2$ and 27.75 mol of water, corresponding to total solids = 3.25 mol and 500 g water. The amount of calcite relative to other phases has been selected to be just sufficient to achieve calcite saturation at 0 °C. C–S–H is not considered in the calculations. The authors are aware of possible AFt–AFm mass balance changes due to sulfate and aluminium incorporation into C–S–H. However the currently available dataset is not complete and therefore does not allow us to draw final conclusions regarding the impact of ion substitution in C–S–H on AFt-AFm phase assemblages. We think that C–S–H which is abundant in commercial cements will mainly dilute the volume changes arising from phase changes occurring as a function of reactions between portlandite, AFt, AFm and water.

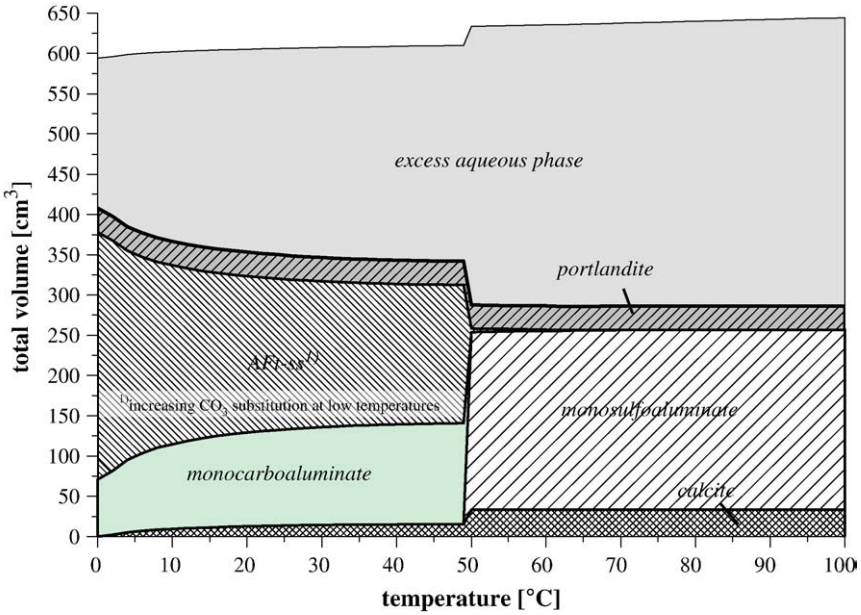

Fig. 11. Influence of temperature on specific volume changes of hydrate phases of a hydrated model mixture consisting of C_3A, portlandite, $CaSO_4$ and $CaCO_3$; fixed sulfate ratio ($SO_3/Al_2O_3 = 1$) and carbonate ratio ($CO_2/Al_2O_3 = 1.25$) (constant total amount of solids, $C_3A + CaSO_4 + CH + Cc = 3.25$ mol, reacted with 500 g water).

The calculation was repeated for this composition using small increments of temperature, equilibrium being assumed at each step, with the results shown in Fig. 11. Hydration at 0 °C results in three solid phases coexisting with an aqueous phase; monocarboaluminate, portlandite and an SO_4–CO_3-ettringite-type solid solution. With rising temperature, and assuming equilibrium is maintained, the stable range of ettringite solid solutions will contract. As a consequence, free calcite appears as the temperature increases. This process results in decreasing amounts of AFt and creation of two solids: calcite and CO_3-AFm, as well as increasing mass of the aqueous phase. As a consequence of the changing phase balances, a significant diminution in specific volume of the solids will occur with rising temperature. This diminution does not occur as a step at a particular temperature but is instead distributed over a range of temperatures, although the intensity of the calcite-shedding process will be greatest in the low-temperature range *ca* 0–20 °C. The amount of monocarboaluminate also increases rapidly to accommodate some of the carbonate expelled from ettringite solid solutions No further significant phase changes occur up to 48 °C, at which temperature both monocarboaluminate and ettringite become unstable and monosulfoaluminate has close to its ideal composition. The changes depicted with rising temperature are reversible, so that the sequence of reaction with falling temperature is the opposite of that described and, of course, with reversed direction of changing solid volume.

Thus the calculations (Fig. 11) show that if a calcite-saturated cement is set under warm conditions, but is subsequently used in cold conditions (probably a more commonly-encountered thermal cycle than the sequence with rising temperature presented above, because

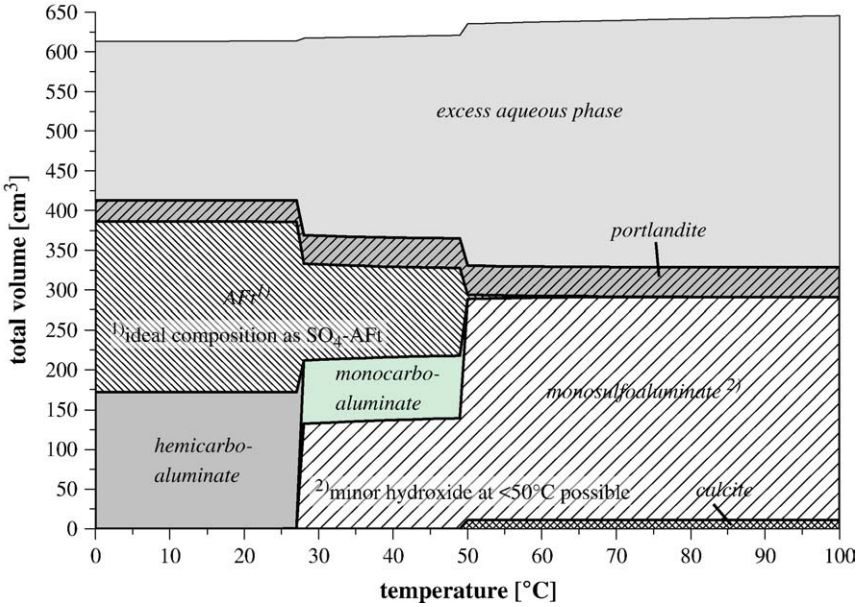

Fig. 12. Influence of temperature on specific volume changes of hydrate phases of a hydrated model mixture consisting of C_3A, portlandite, $CaSO_4$ and $CaCO_3$; fixed sulfate ratio ($SO_3/Al_2O_3 = 1$) and carbonate ratio ($CO_2/Al_2O_3 = 0.33$) (constant total amount of solids, $C_3A + CaSO_4 + CH + Cc = 3.25$ mol, reacted with 500 g water).

of the exothermic nature of cement hydration), this sequence of phase and volume changes will lead to uptake of carbonate and water into solids with increase in solids volume. The quantitative increase in solid volume will be much greater if initial set occurred above 48 °C than below. Of course the calculations assume equilibrium conditions. However the calculation shows that the thermodynamic driving force of formation of monosulfoaluminate, rather than monocarboaluminate, increases with increasing temperatures >48 °C. Also, the calculation of volume changes presented here is simplified insofar as it does not include a correction for the normal thermal dilatational coefficients of the solids, although the correction is believed to be small relative to the combined impacts of phase change and changing extent of solid solution.

The role of carbonate in controlling the specific volume of solids is further illustrated by considering a composition with much lower carbonate ratio, 0.33, than was used in the previous calculation set. Fig. 12 shows the results calculated for a model cement comprised of 0.907 mol each of C_3A and $CaSO_4$, 0.30225 mol $CaCO_3$, 1.13375 mol of portlandite and 27.75 mol water. Under the conditions imposed on calculation, free calcite will only appear at temperatures above 48 °C; at lower temperatures, carbonate will be entirely contained in the AFm phase, as either (or both, depending on temperature) mono- and hemicarboaluminate. Because the carbonate activity decreases at <48 °C to below the calcite saturation threshold, relatively little carbonate will be able to enter AFt, even at 0 °C, and, as a consequence, the significant volume changes now become concentrated in two steps, one occurring about 27 °C and the other about 48 °C. The impacts of heating and cooling on the specific volume of solids can be assessed as shown for the previous example and it will be seen that many features differ significantly as a consequence of the apparently minor change in composition. For example, on account of the low carbonate activity (which we may equate with a low carbonate ratio), the opportunity for carbonate incorporation into ettringite greatly diminishes despite low temperatures, <20 °C, and one source of potential change in the specific volume of solids is thereby reduced or eliminated.

The relations between temperature, paste composition and mineralogy may in part account for the frequent assertions in the literature that the total porosity of cement paste increases with rising cure temperatures (see also [3] for more information). As AFt changes in composition and solubility with rising temperature, this normally results in diminishing amounts of AFt. Unless physical shrinkage can occur, the specific volume of solids will be less able completely to fill space and porosity will increase.

4. Discussion

The conventional picture of Portland cement compositions is that the mineralogy of the cement paste, as known for about 25 °C is persistent but that curing at higher temperatures, above 40 °C or thereby, significantly alters the 25 °C mineralogy. The present study shows that this conclusion is broadly true for carbonate-free cements, the instability of hydrogarnet at lower temperatures, <8 °C, and the changing SO_4/OH ratio of monosulfoaluminate solid solutions being a notable exception. However many cements are either made with added limestone (itself comprised mainly of calcite), or else gain carbonate in service, or both, and a rather different picture emerges about the impact of temperature on the mineralogy of cements if carbonate is considered.

The activity of carbonate in Portland cement is conditioned by three thresholds: (i) by the equilibrium between C_4AH_x and hemicarboaluminate, (ii) by the equilibrium between hemi- and monocarboaluminate and (iii), by the equilibrium between monocarboaluminate and calcite. Thus we have three principal states to assess with respect to the role of carbonate. Assemblage (i) may not be important to commercial cements as it is formed only at very low total carbonate content. In cements which contain intrinsic carbonate [35], added limestone, or exposed to air, states (ii) or more likely , (iii), can be regarded as the normal condition at 25 °C. As a good approximation, the carbonate activity of a calcite-saturated cement paste is therefore essentially fixed at constant temperature by the coexistence of calcite and monocarboaluminate.

The buffering action of the carbonate pairs is a great simplification with respect to defining the envelope of conditions in which the paste mineralogy is constant, leaving us free to concentrate on the impacts of changing temperature. Similarly, we have described the buffering reactions which govern the solubility of sulfate. And of course the hydroxide activity, expressed in terms of the pH function, is fixed by the coexistence of portlandite with other cement phases. Thus the numerical values of the activities of anionic species (hydroxide, sulfate, carbonate) are temperature dependent but in a predictable way. We thus have a temperature-dependent envelope of species activities (carbonate, sulfate and hydroxide) in which cement hydration can occur. The boundaries of this envelope are rather sharply constrained by the considerations outlined above. Thus, while the possibilities for variation within the envelope are in theory infinite, in practice, they are sufficiently constrained by phase rule and boundary conditions that we have only a few cases to consider with respect to the *number and mineralogical identity* of the phases present, the analysis presenting an infinity of solutions only if we consider the *amount* of phases.

We can apply this reasoning to the constitution of other phases present in the hydrated paste and as a result, achieve simplification. For example, portlandite does not incorporate carbonate, sulfate or hydroxide with respect to its normal stoichiometry. Likewise, C–S–H incorporates relatively little sulfate or alumina with respect to its normal stoichiometry within the envelope of conditions outlined previously: the limits of sulfate and alumina incorporation in C–S–H will be provided by Skapa and Glasser [34]. But given the abundance of C–S–H in hydrated paste, it is desirable to correct the sulfate and alumina contents to calculate that which is available for AFm and AFt formation. A consequence of these balances is that significant changes can occur amongst the AFm and AFt phases probably without affecting the nature of the C–S–H phase. For these reasons, C–S–H and $Ca(OH)_2$ can be omitted from many of the diagrams shown here: once saturated, they behave as “passengers” or inert diluents. There are of course limits to the inertness of C–S–H, for example when thaumasite becomes stable; these conditions will be explored in a subsequent paper [31]. However thaumasite is not predicted to occur in fresh or mature cement pastes in service environments with low sulfate and carbonate concentrations. Questions about the stability limits of hydrogarnet have also been resolved, although only tentatively but it is useful to note that the “conversion” problem which affects aluminate cements is unlikely to be a problem in Portland cements except at high temperatures and low sulfate contents.

The changing phase relations with temperature and species activities can be treated as describing and quantifying a competition for anion sites between hydroxide, carbonate and sulfate, the hosts being almost entirely AFm, AFt or mixtures of the two, except for minor incorporation in C–S–H. This competition is constrained by the phase rule and by mass balances, including available alumina enabling us for example, to make extensive use of the carbonate and sulfate (to alumina) ratios to predict paste mineralogy. Some generalisations are possible: higher temperatures, >25 °C, stabilise SO_4-AFm with respect to OH-AFm and OH-substituted sulfate AFm. Lower temperatures, <25 °C, favour increasing replacement of sulfate in AFm by hydroxide and carbonate. This substitution is partly gradual but incomplete: solid solution may require phase changes so, depending on composition and temperature, several discrete AFm phases may coexist with each other as well as with AFt. However, rather different trends are encountered for AFt. It is probable that within the envelope of conditions depicted here, relatively little OH is substituted into

(SO_4, CO_3) AFt, because (i) a divalent anion gives better local charge compensation on anion sites (ii) spatial requirements: two OH groups are difficult to fit onto a sulfate site because to our knowledge, occupancy of other sites does not confer stability on the atomic arrangement. However with decreasing temperature, carbonate—with the same charge as sulfate—is increasingly stabilised in AFt. Theoretically, these AFt substitutions do not require a phase change, at least up to 50 mol% replacement in the ettringite structure: the maximum carbonate activity achieved by calcite is insufficient to stabilise CO_3-AFt even at 0 °C.

Taken together, these trends are responsible for the rich and varied patterns of the coexistence of AFm and AFt phases with temperature as described here. The complex temperature dependence of anion stabilisation energies within AFm and AFt structures would be a fascinating subject for the application of molecular modelling.

Calculation also reveals temperature-dependent differences in the amount of water bound into solids. While we have not determined the temperature dependence of the water content of C–S–H, which will also impact on the overall amount of bound water, a generic conclusion is that the bound water content of cement paste will increase markedly at low temperatures. This increase is connected with the amount of ettringite, the ability of which to combine water exceeds that of other cement hydrates. The low physical density of AFt contributes to better space filling and, in turn, increasing AFt helps create a matrix with lower porosity. Many sophisticated theories have been advanced concerning the characterisation and role of the pore network and total porosity in cement pastes and its relation to permeability but it is refreshing to find that very simple considerations, such as the specific volume occupied by solids, can give valuable guidance to the changes in permeation properties of hardened paste. Also, that depending on composition, the space filling may be sensitive to relatively small changes in composition and to small increments of temperature; this is discussed in general terms subsequently.

The present study discloses that the amount of calcite potentially able to react with cement increases rapidly with decreasing temperature, especially both below 20 °C and at low sulfate ratios. Thus, while an excess of calcite may persist in pastes cured in warm conditions, the excess may become reactive at lower temperatures where an important reaction enabling calcite partially to replace sulfate in ettringite affects calcite consumption. This, in turn, introduces the possibility that the internal constitution of a cement paste could differ significantly depending upon service temperatures and thermal history, with calcite reacting in cold conditions but exsolving from ettringite in warm conditions. However the kinetics of calcite dissolution and of nucleation and precipitation within the paste matrix, and attendant changes in microstructure, are not as yet sufficiently well established to venture predictions about the impacts of these processes on the mechanical and physical properties of the paste. Present and incomplete data show that carbonate equilibria are attained rapidly, within weeks or months, with falling as well as with rising temperatures. Indeed a range of conditions need eventually to be considered but it is predicted that the most distinctive differences achieved by carbonate additions will be encountered when comparing mineralogy and microstructure of cement paste, either plain or carbonate filled, in four different regimes.

- Set and hardened at low temperature, perhaps in the range of 0 to 5 °C, which does not vary significantly thereafter: this is considered to be a benchmark case.
- Set and hardened at low temperature but thereafter, perhaps on an annual basis, the temperature fluctuates between cold, ~1–5 °C, and warm, ~30 °C or more.
- Set and hardened under "warm" conditions, 25 °C or more, but thereafter, the cement is continuously exposed to cold conditions.
- Set and hardening occur under "warm" conditions but service temperatures fluctuate between cold and warm, perhaps seasonally.

Both static (bullet point 1) and dynamic conditions (bullet points 2–4) are important; bullet point 3 is especially relevant to concretes which experience self-heating during initial hydration but thereafter are used in cold climates.

To realise the consequences of the low temperature reactivity of carbonate, we envisage four important remaining tasks. These are (i) to quantify differences in physical microstructure and space filling of calcite-filled cement as functions of hydration temperature and to determine the consequences of thermal cycling in the range of anticipated service conditions (ii) to determine directly the impacts of (i) on porosity, permeability and strength, (iii) to investigate the kinetics of temperature-dependent processes involving solid phase dissolution and precipitation and (iv) to verify the limits of calcite solid solution in AFt and verify experimentally the influence of higher sulfate concentration on suppressing carbonate uptake of ettringite. The latter experiments, (iv), are in progress and have now been reported [30].

The results of the present study also affect our understanding of delayed ettringite formation (DEF). Previous studies have focussed on a "safe" upper limit for warm cure. Our calculations do not disagree concerning the impact of elevated temperature. However they also show that the lower temperature, at which cements and concretes are used in the post warm cure regime, affects the potential for expansion, with large differences expected in the rather narrow range of temperature between 0 and 25 °C, and the biggest impact expected for lower temperatures, close to 0 °C.

The impacts of alkali on the phase development have not been assessed in detail. However we venture some comments. As alkali is added to cement, the OH ions contributed by sodium and potassium approximately balance the loss of OH resulting from diminution of calcium (hydroxide) solubility. This regime extends up to (Na,K) concentrations ~30–40 mM at 25 °C, with the result that pH increases only slightly over this range. Sulfate solubility does rise, but only slightly, with the result that cation charges continue to be balanced mainly by OH. This means that the competition for anion sites in AFm and AFt is also unaffected, or nearly so, by low alkali concentrations. However at higher alkali contents, aqueous OH concentrations rise rapidly; but SO_4 concentrations rise even more rapidly. As the pH increases to >13, we lack adequate experimental data about limits of solid solution etc. and are less confident about activity-composition corrections. Moreover, the distribution model we use will have to be rewritten to accommodate ternary solid solution, to allow for multiple anion substitution (sulfate, hydroxide and carbonate) in the same phase. The existence of another AFm, the so-called U phase [36], has been reported at high sodium contents,>0.5 M, suggesting that another set of partition functions would also have to be developed for the coexistence of "U" with other phases.

We also point to the need for additional studies, especially the sensitivity of reaction to the source of carbonate. We consider mainly carbonate arising from calcite but equally the carbonate may arise from atmospheric carbon dioxide, or be delivered in solution, in natural waters, or in several of these ways. These two sources, calcite or CO_2, have different impacts on mass balances but probably the most significant factor not yet included in the scope of work is the lowered pH encountered in partially carbonated cement paste. The calculations presented here would need to be redone for portlandite-free systems in order to assess the potential for changes in all but the earliest stages of carbonation.

However an inescapable conclusion arising from the title study is that phase changes relative to cement performance are not confined to elevated temperatures: important changes may also occur in the low temperature range and are not restricted to the formation of thaumasite and related phase assemblages. Elucidating these changes becomes easier as we enter an era of quantification of paste mineralogy. Calculations described here enable us to assess the impact of reactive admixtures, as has been done for calcite. The results of calculation still need to be subject to practical assessment—some of

which is in progress—but undertaking calculations, as has been done here, highlights the factors critical to performance and thereby focuses practical testing and assessments. The challenges to the industry are numerous and varied but what is certain is that we cannot wait decades for results of tests on the performance of modified cements but neither can we trust experience or intuition: calculation is increasingly seen as a way forward.

Acknowledgements

The work performed here was supported by NANOCEM, a research consortium of European cement producers and academic institutions. The studentship provided to one of us (T.M.) has enabled him to successfully complete his PhD and enter cement research at Holcim Group Support Ltd., Switzerland. We also thank EMPA (Switzerland) and in particular, Dr Barbara Lothenbach, who provided work experience in a different environment and for helpful discussion.

References

[1] Internal Sulfate Attack and Delayed Ettringite Formation, in: K. Scrivener, J. Skalny (Eds.), Proceedings of the International RILEM TC 186-ISA Workshop, RILEM publications, Paris, 2004.
[2] T. Matschei, B. Lothenbach, F.P. Glasser, Thermodynamic properties of Portland cement hydrates in the system $CaO–Al_2O_3–SiO_2–CaSO_4–CaCO_3–H_2O$, Cement and Concrete Research 37 (2007) 1379–1410.
[3] B. Lothenbach, T. Matschei, G. Möschner, F.P. Glasser, Thermodynamic modelling of the effect of temperature on the hydration and porosity of Portland cement, Cement and Concrete Research 38 (2008) 1–18.
[4] T. Matschei, B. Lothenbach, F.P. Glasser, The AFm phase in Portland cement, Cement and Concrete Research 37 (2007) 118–130.
[5] T. Matschei, B. Lothenbach, F.P. Glasser, The role of calcium carbonate in cement hydration, Cement and Concrete Research 37 (2007) 551–558.
[6] T. Matschei, F.P. Glasser, Zum Einfluss von Kalkstein auf die Zementhydratation, Zement Kalk Gips 59 (12/2006) 78–86.
[7] T. Matschei, R. Skapa, B. Lothenbach, F.P. Glasser, The distribution of sulfate in hydrated Portland cement paste, Proceedings of the 12th Intern. Congress on the Chemistry of Cements, Montreal, 2007.
[8] T. Matschei, D. Herfort, B. Lothenbach, F.P. Glasser, Relationships of Cement Paste Mineralogy to Porosity and Mechanical Properties, Modelling of Heterogenous Materials with Applications in Construction and Biomedical Engineering, Prague, 2007 extended abstract.
[9] Kulik, D.; Berner, U.; Curti, E.: Modelling chemical equilibrium partitioning with the GEMS-PSI code. PSI Scientific Report 2003, Vol. IV, 109–122, http://gems.web.psi.ch.
[10] Thönen, T.; Kulik, D. Nagra/PSI Chemical Thermodynamic Data Base 01/01 for the GEM-Selektor (V.2-PSI) Geochemical Modeling Code: Release 28-02-03. PSI Technical Report TM-44-03-04 (unpublished) about the GEMS version of Nagra/PSI chemical thermodynamic database 01/01. 2003.
[11] W. Hummel, U. Berner, E. Curti, F.J. Pearson, T. Thönen, Nagra/PSI Chemical Thermodynamic Data Base 01/01, Universal Publishers, Parkland, Florida, USA, 2002.
[12] J.W. Johnson, E.H. Ölkers, H.C. Helgeson, SUPCRT92: a software package for calculating the standard molal thermodynamic properties of minerals, gases, aqueous species, and reactions from 1 to 5000 bar and 0 to 1000 °C, Computers & Geosciences 18 (1992) 899–947 slop98.dat database available from http://geopig.asu.edu/supcrt92_data/slop98.dat.
[13] E.L. Shock, D.C. Sassani, M. Willis, D. Sverjensky, Inorganic species in geologic fluids: correlations among standard molal thermodynamic properties of aqueous ions and hydroxide complexes, Geochimica et Cosmochimica Acta 61 (1997) 907–950.
[14] D. Sverjensky, E.L. Shock, H.C. Helgeson, Prediction of the thermodynamic properties of aqueous metal complexes to 1000 °C and 5 kbar, Geochimica et Cosmochimica Acta 61 (1997) 1359–1412.
[15] V.I. Babushkin, G.M. Matveev, O.P. Mčedlov-Petrosjan, Thermodinamika Silikatov, Springer, Moskau, 1985.
[16] Glynn P.: Solid-solution Solubilities and Thermodynamics: Sulfates, Carbonates and Halides. In: Sulfate Minerals: Crystallography, Geochemistry and Environmental Significance, Alpers C.N., Jambor J.L. and Nordstrom D.K. (eds.), Mineralogical Society of America and Geochemical Society, Reviews in Mineralogy and Geochemistry, 2000, v. 40, 481–511.
[17] P.D. Glynn, MBSSAS: a code for the computing of margules parameters and equilibrium relations in binary solid-solutions aqueous-solution systems, Computers & Geoscience 17 (1991) 907–966.
[18] T. Matschei, F.P. Glasser, Interactions between Portland cement and carbon dioxide, Proceedings of the 12th ICCC, Montreal, 2007.
[19] Midgley, H.G.; Rosaman, D.: The composition of ettringite in set Portland cement. Proceedings of the IV. Intern. Symposium on the chemistry of Cements, Washington, D.C, 1964, Vol. III-S2 p. 259–262.
[20] J. Neubauer, F. Götz-Neunhöffer, D. Schmitt, M. Degenkolb, U. Holland, In-situ Untersuchung der frühen PZ-Hydratation. Proceedings of the 16th Ibausil, Weimar, 2006, Vol. I, 1-0375 – 1-0382.
[21] C.J. Warren, E.J. Reardon, The solubility of ettringite at 25 °C, Cement and Concrete Research 24 (1994) 1515–1524.
[22] H. Pöllmann, H.J. Kuzel, R. Wenda, Solid solution of ettringites part I: incorporation of OH^- and CO_3^{2-} in $3CaO·A1_2O_3·3CaSO_4·32H_2O$, Cement and Concrete Research 20 (1990) 941–947.
[23] S.J. Barnett, C.D. Adam, A.R.W. Jackson, An XRPD profile fitting investigation of the solid solution between ettringite, $Ca_6Al_2(SO_4)_3(OH)_{12}·26H_2O$, and carbonate ettringite, $Ca_6Al_2(CO_3)_3(OH)_{12}·26H_2O$, Cement and Concrete Research 31 (2001) 13–17.
[24] E.T. Carlson, H.A. Berman, Some observations on the calcium aluminate carbonate hydrates, Journal of Research of the National Bureau of Standards 64 (1960) 333–341.
[25] E.P. Flint, L.S. Wells, Analogy of hydrated calcium silicoaluminates and hexacalcium aluminate to hydrated calcium sulfoaluminates, Journal of Research of the National Bureau of Standards 33 (1944) 471–478.
[26] J. Murdoch, Crestmore past and present, American Mineralogist 46 (1961) 245–257.
[27] J. Murdoch, R.A. Chalmers, Ettringite ("woodfordite") from Crestmore, American Mineralogist 45 (1960) 1275–1278.
[28] H. Kollmann, G. Struebel, Ettringite-Thaumasit-Mischkristalle von Brenk (Eifel), Chemie der Erde 40 (1981) 110–120.
[29] T. Matschei, F.P. Glasser, New Approaches to Quantification of Cement Hydration, Proceedings of the 16th Ibausil, Weimar, vol. I, 2006, 1-0389–1-0400.
[30] T. Matschei, F.P. Glasser, Phase Assemblages Relevant to Portland Cement Hydration at Low Temperatures, 0–25 °C, Proceedings of the 17th Ibausil, Weimar, vol. I, 2009, 01-219–01-233.
[31] T. Matschei, D. Macphee, F.P. Glasser, in preparation 2009.
[32] H. Pöllmann, Solid solution in the system $3CaO\ Al_2O_3\ CaSO_4$ aq – $3CaO\ Al_2O_3\ Ca(OH)_2$ aq, Neues Jahrbuch fuer Mineralogie Abhandlungen 161 (1989) 27–41.
[33] M.H. Roberts, Calcium aluminate hydrates and related basic salt solid solutions, Proceedings of the V. Intern. Symposium on the Chemistry of Cements, Tokyo, vol. II, 1969, pp. 104–117.
[34] R. Skapa, F.P. Glasser, in preparation 2009.
[35] T.I. Barry, F.P Glasser, Calculation of Portland cement clinkering reactions, Advances in Cement Research 12 (2000) 19–28.
[36] W. Dosch, H. zur Strassen, Ein alkalihaltiges Calciumaluminatsulfathydrat (Natrium-Monosulfat), Zement-Kalk-Gips 20 (9) (1967) 392–401.
[37] H. Strunz, H.E. Nickel, Mineralogical Tables, 9th EditionE. Schweizerbart'sche Verlagsbuchhandlung, Stuttgart, 2001.